

## Modeling, Calculating, and Analyzing Multidimensional Vibrational Spectroscopies

YOSHITAKA TANIMURA\* AND AKIHITO ISHIZAKI†

Department of Chemistry, Graduate School of Science, Kyoto University  
Kitashirakawa, Sakyo, Kyoto 606-8502, Japan

RECEIVED ON FEBRUARY 4, 2009

### CONSPECTUS

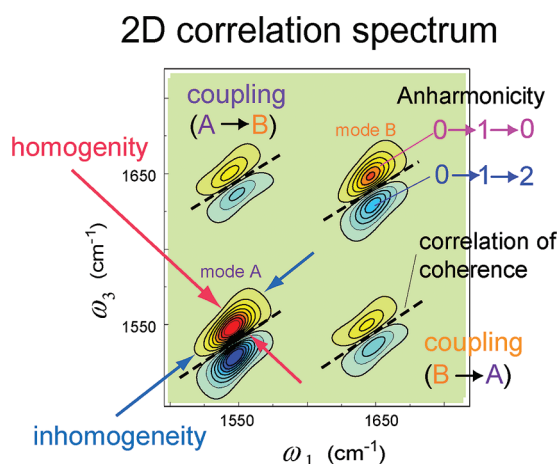
Spectral line shapes in a condensed phase contain information from various dynamic processes that modulate the transition energy, such as microscopic dynamics, inter- and intramolecular couplings, and solvent dynamics. Because nonlinear response functions are sensitive to the complex dynamics of chemical processes, multidimensional vibrational spectroscopies can separate these processes. In multidimensional vibrational spectroscopy, the nonlinear response functions of a molecular dipole or polarizability are measured using ultrashort pulses to monitor inter- and intramolecular vibrational motions. Because a complex profile of such signals depends on the many dynamic and structural aspects of a molecular system, researchers would like to have a theoretical understanding of these phenomena.

In this Account, we explore and describe the roles of different physical phenomena that arise from the peculiarities of the system—bath coupling in multidimensional spectra. We also present simple analytical expressions for a weakly coupled multimode Brownian system, which we use to analyze the results obtained by the experiments and simulations.

To calculate the nonlinear optical response, researchers commonly use a particular form of a system Hamiltonian fit to the experimental results. The optical responses of molecular vibrational motions have been studied in either an oscillator model or a vibration energy state model. In principle, both models should give the same results as long as the energy states are chosen to be the eigenstates of the oscillator model. The energy state model can provide a simple description of nonlinear optical processes because the diagrammatic Liouville space theory that developed in the electronically resonant spectroscopies can easily handle three or four energy states involved in high-frequency vibrations.

However, the energy state model breaks down if we include the thermal excitation and relaxation processes in the dynamics to put the system in a thermal equilibrium state. The roles of these excitation and relaxation processes are different and complicated compared with those in the resonant spectroscopy. Observing the effects of such thermal processes is more intuitive with the oscillator model because the bath modes, which cause the fluctuation and dissipation processes, are also described in the coordinate space. This coordinate space system—bath approach complements a realistic full molecular dynamics simulation approach.

By comparing the calculated 2D spectra from the coordinate space model and the energy state model, we can examine the role of thermal processes and anharmonic mode—mode couplings in the energy state model. For this purpose, we employed the Brownian oscillator model with the nonlinear system—bath interaction. Using the hierarchy formalism, we could precisely calculate multidimensional spectra for a single and multimode anharmonic system for inter- and intramolecular vibrational modes.



### I. Introduction

Spectral line shapes in a condensed phase contain information from various dynamic processes, including such important processes as microscopic dynamics, inter- and intramolecular couplings, and solvent dynamics, all of which modulate the transition energy.<sup>1</sup> Energy and phase relaxations as

well as thermal excitations take place whenever a system is affected by coupling to other degrees of freedom and the resultant line shape from molecules in the condensed phase is broadened and overlapped.<sup>2</sup> Due to the sensitivity of nonlinear response functions to complex dynamics, multidimensional vibrational spectroscopies are capable

of separating the above-mentioned processes. Fifth-order two-dimensional (2D) Raman<sup>3–6</sup> and third-order 2D infrared (IR) spectroscopies<sup>7–10</sup> are such examples. The fifth-order Raman response is represented by the three-body correlation function of polarizability,  $\Pi$ , whereas the third-order IR response is represented by the four-body correlation function of dipole,  $\mu$ . They are expressed as<sup>1,2</sup>

$$R_{\text{Raman}}^{(5)}(t_2, t_1) = -\frac{1}{\hbar^2} \langle [[\Pi(\hat{\mathbf{q}}(t_{12})), \Pi(\hat{\mathbf{q}}(t_1)), \Pi(\hat{\mathbf{q}})] \rangle \quad (1)$$

and

$$R_{\text{IR}}^{(3)}(t_3, t_2, t_1) = -\frac{i}{\hbar^3} \langle [[[\mu(\hat{\mathbf{q}}(t_{123})), \mu(\hat{\mathbf{q}}(t_{12})), \mu(\hat{\mathbf{q}}(t_1)), \mu(\hat{\mathbf{q}})] \rangle \quad (2)$$

where we denote the set of molecular coordinates by  $\hat{\mathbf{q}} = (\hat{q}_1, \hat{q}_2, \hat{q}_3, \dots)$  and set  $t_{12} \equiv t_1 + t_2$  and  $t_{123} \equiv t_1 + t_2 + t_3$ . The Hamiltonian for the vibrational modes is expressed in the molecular coordinate  $\hat{q}_i$  as the coupled oscillators by

$$H_A = \sum_i \left( \frac{1}{2} \hat{p}_i^2 + U_i(\hat{q}_i) \right) + \sum_{ij} U'(\hat{q}_i, \hat{q}_j) + \sum_{ij,k} U''(\hat{q}_i, \hat{q}_j, \hat{q}_k) + \dots \quad (3)$$

where  $U_i(\hat{q}_i)$  is the potential for mode  $i$  and  $U'(\hat{q}_i, \hat{q}_j)$  and  $U''(\hat{q}_i, \hat{q}_j, \hat{q}_k)$  are the anharmonic mode–mode interactions. The optical responses of molecular vibrational motions have been studied theoretically in either a molecular coordinate or a vibrational energy state representation.<sup>1</sup> The coordinate representation is physically intuitive since the optical observables (the dipole moments,  $\mu(\hat{\mathbf{q}})$ , or the Raman polarizabilities,  $\Pi(\hat{\mathbf{q}})$ ) are also described by the molecular coordinates. The energy state representation employs the energy eigenfunctions of a molecular motion and is physically equivalent to the oscillator model in the coordinate representation. Accordingly, laser interactions are described by the transitions between the energy states, and the optical processes, including the time ordering of the laser pulses, are conveniently described by diagrams such as the double-sided Feynman diagrams.<sup>1,2</sup> The energy-state model has the advantage of identifying peak positions of the optical signals in the frequency domain, since the peaks appear as the transition between the energy states.

Although dynamics does not change regardless of the representation, a difference appears if the thermal excitation and relaxation processes are included into the system dynamics to have the thermal equilibrium in a certain time period. To illustrate this point, we consider the bath Hamiltonian described by the bath mode  $\hat{x}_{\alpha_i}$  that is attached to the system as  $\hat{H}_{\text{tot}} = \hat{H}_A + \hat{H}_B$ , where

$$\hat{H}_B = \frac{1}{2} \sum_i \sum_{\alpha_i} \left[ \hat{p}_{\alpha_i}^2 + \omega_{\alpha_i}^2 \left( \hat{x}_{\alpha_i} - \frac{c_{\alpha_i} V(\hat{q}_i)}{\omega_{\alpha_i}^2} \right)^2 \right] \quad (4)$$

The system–bath interaction is assumed to be linear plus square in the system coordinate as  $V(\hat{q}_i) = \xi_{\text{LL}} \hat{q}_i + \xi_{\text{SL}} \hat{q}_i^2/2$ , but linear in the bath coordinates.<sup>11–13</sup> The coupling to the bath can be interpreted as the anharmonic interaction to the optically inactive modes. As shown in Figures 1 and 2, while the linear–linear interaction (LL) mainly contributes to energy relaxation, the square–linear (SL) system–bath interaction leads to the vibrational dephasing for the slow modulation case due to the frequency fluctuation of system vibration.<sup>14–19</sup>

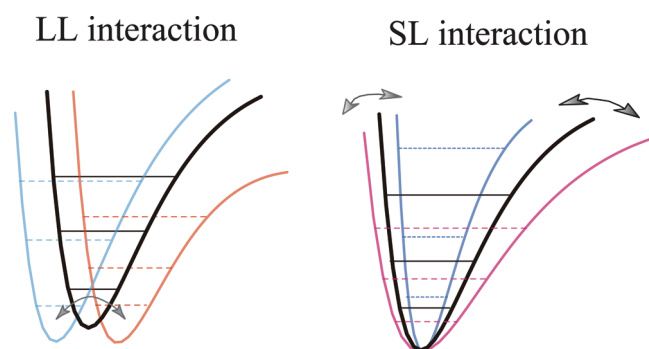


**FIGURE 1.** Schematic illustrations of the effects of the linear–linear (LL) and the square–linear (SL) system–bath couplings on a Morse potential system. The black lines represent the unperturbed potential, while the colored lines represent the perturbed one. The LL coupling swings the position of the potential, whereas the SL coupling shakes the potential surface. Due to the anharmonicity of the potential, the LL interaction deforms the potential inducing a slight frequency fluctuation.

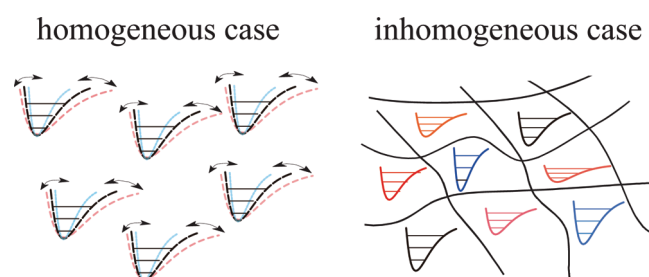


**FIGURE 2.** Schematic views of homogeneous (fast-modulation limit) and inhomogeneous (slow-modulation limit) distributions of the potential system perturbed by the SL system–bath interaction.

This can be seen by introducing the energy eigenstate representation of  $\hat{H}_A$  expressed by  $|n_i\rangle$  for eigenvalue  $\hbar\omega_{n_i}/2$  and by expressing the SL interaction as  $\hat{q}_i^2 \sum_{\alpha_i} c_{\alpha_i} \xi_{\text{SL}} \hat{x}_{\alpha_i} \rightarrow \hat{q}_i^2 X_i(t)$ , where  $X_i(t)$  is the noise induced by the bath oscillators. If we neglect the dissipation and only consider the fluctuation arising from the SL interaction, the effective Hamiltonian,  $H'_A(t)$  is expressed as<sup>2</sup>

$$H'_A(t) = \frac{\hbar}{2} \sum_i \sum_{n_i} [\omega_{n_i} + \delta\Omega_{n_i}(t)] |n_i\rangle \langle n_i| + \sum_{ij} \sum_{n_i m_j} U'_{n_i m_j} |n_i\rangle \langle m_j| + \dots \quad (5)$$

where  $\delta\Omega_{n_i}(t) = 2X_i(t)\langle n_i|\hat{q}_i^2|n_i\rangle/\hbar$  is the frequency fluctuation induced by the bath modes. This is the commonly used Hamiltonian to account for the vibrational dephasing and the frequency fluctuations are treated in the framework of the multistate stochastic theory.<sup>20–28</sup> We should notice that the bath effects consist of the fluctuation and dissipation parts, both of which ensure the thermal equilibrium state of the entire system through the fluctuation–dissipation theorem. This stochastic model neglects the dissipation part of the bath effects and does not reach the thermal equilibrium state as the steady state.<sup>2</sup> However, it turns out that the stochastic model explains the high-frequency intramolecular vibrational mode very well for the slow modulation case (vibrational dephasing case) as shown in section II.<sup>18</sup>

While the mechanisms as well as the effects of thermal processes is not clear in the stochastic energy state model, it is more intuitive to see the oscillator model represented by the coordinate, since the bath modes, which cause the excitation and relaxation processes, are also described in the coordinate space. This coordinate space system–bath approach is also complementary to a realistic full molecular dynamics simulation approach. In this Account, we explore and clarify the roles of different physical phenomena arising from the peculiarities of the system–bath coupling via the multidimensional spectra. We also present simple analytical expressions for a weakly coupled multimode Brownian system because they are convenient to analyze the results obtained by the experiments and simulations.

## II. System–Bath Approach and Stochastic Approach to Intramolecular Vibrational Mode

The validity of the oscillator model was assessed by comparing the 2D signals calculated from the total Hamiltonian,  $\hat{H}_{\text{tot}} = \hat{H}_A + \hat{H}_B$ , and from the effective stochastic Hamiltonian,  $H'_A(t)$ , for a single mode case. While the spectra for the effective Hamiltonian  $H'_A(t)$  are calculated from the multistate stochastic theory using the Liouville space response function, the exact spectra for the total Hamiltonian,  $\hat{H}_{\text{tot}} = \hat{H}_A + \hat{H}_B$  are obtained by solving the reduced equation of motion. The character of the bath is determined by the spectral distribution of the system–bath interaction,  $J(\omega)$ . If we set  $J(\omega) \propto \omega\gamma^2/(\gamma^2 + \omega^2)$ , the thermal fluctuation induced by the bath exhibits a sto-

chastic Gaussian–Markovian modulation defined by  $\langle \delta\Omega(t')\delta\Omega(t'') \rangle \propto \exp[-\gamma(t' - t'')]$ , in which  $\gamma$  corresponds to the inverse correlation time of the noise.<sup>2</sup> As was shown by Tanimura et al., such a dissipative system can be treated by utilizing a tridiagonal hierarchy of equations (the Gaussian–Markovian quantum Fokker–Planck equations).<sup>29,30</sup> For a low temperature case, the structure of hierarchy becomes complicated because of the quantum nature of the heat bath characterized by Matsubara frequencies.<sup>31–33</sup> However there is a rigorous but simple way to terminate the hierarchy, by reducing the quantum Fokker–Planck equation with low-temperature correction terms.<sup>34</sup> The key to calculate the nonlinear response functions is the quantum coherence between the system and the bath, which plays an essential role for strong system–bath coupling.<sup>35</sup> Up to now, only the hierarchy equation approach could handle the quantum dynamics for nonlinear response functions under the strong coupling at low temperature without the rotating wave approximation. We employ the same parameters given in ref 18 and describe a high-frequency intramolecular vibrational mode by the Morse oscillator  $U_A(q) = \hbar\omega_A[1 - \exp(-\alpha_A q)]^2/(2\alpha_A^2)$  with  $\omega_A = 1616 \text{ cm}^{-1}$  and  $\alpha_A = 0.1$ , and the LL and SL coupling strengths,  $\xi_{\text{LL}} = 0.05\omega_A$  and  $\xi_{\text{SL}} = 0.05\omega_A$ , respectively. Throughout this Account, the vibrational coordinate  $q$  is dimensionless, and the temperature is set to be  $T = 300 \text{ K}$ . Then we consider the fast modulation (homogeneous) case,  $\gamma^{-1} = 6.6 \text{ fs}$ , and the slow modulation (inhomogeneous) case,  $\gamma^{-1} = 0.66 \text{ ps}$ . The calculated signals are plotted as the 2D correlation IR spectra defined for the positive  $\omega_1$  and  $\omega_3$  by<sup>36–39</sup>

$$I_C(\omega_3, t_2, \omega_1) = \text{Im}\left\{ \int_0^\infty dt_1 \int_0^\infty dt_3 e^{-i\omega_1 t_1} e^{+i\omega_3 t_3} R_R^{(3)}(t_3, t_2, t_1) \right\} + \text{Im}\left\{ \int_0^\infty dt_1 \int_0^\infty dt_3 e^{i\omega_1 t_1} e^{+i\omega_3 t_3} R_{\text{NR}}^{(3)}(t_3, t_2, t_1) \right\} \quad (6)$$

where  $R_R^{(3)}(t_3, t_2, t_1)$  and  $R_{\text{NR}}^{(3)}(t_3, t_2, t_1)$  are the rephasing and non-rephasing response functions, respectively, and we define the correlation spectra using the opposite sign of the response functions to adapt the commonly used definition. The rephasing response,  $R_R^{(3)}(t_3, t_2, t_1)$ , and the nonrephasing response,  $R_{\text{NR}}^{(3)}(t_3, t_2, t_1)$ , can be separately detected using the phase matching conditions.<sup>40</sup> In the above expressions, the double Fourier transformation entangles absorptive and dispersive contributions to 2D spectra and hence causes the distorted line shape called the phase-twisted line. By adding the two terms corresponding to the rephasing and nonrephasing responses in equal weights, we can remove the dispersive contribution to obtain the pure absorptive line shape. Theoretically, while we can easily separate  $R_R^{(3)}(t_3, t_2, t_1)$  and  $R_{\text{NR}}^{(3)}(t_3, t_2, t_1)$

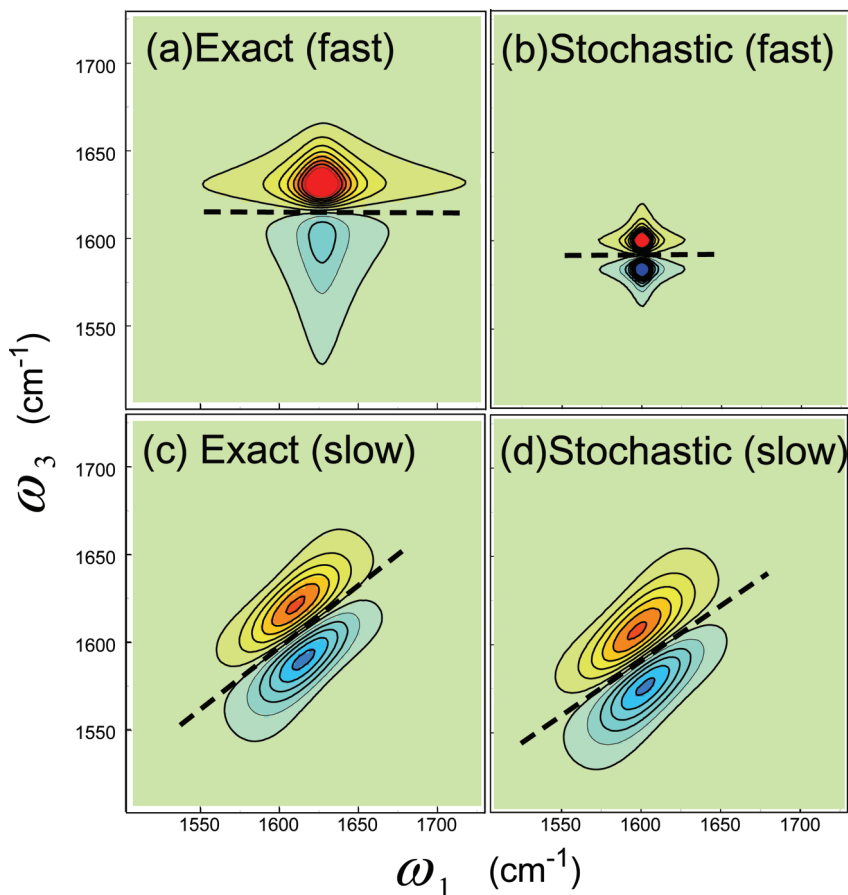


**FIGURE 3.** Two dimensional correlation IR spectra,  $I_C(\omega_3, t_2 = 0, \omega_1)$ , of the Morse oscillator in the motional narrowing regime (a, b), and the dephasing (spectral diffusion) regime (c, d).<sup>18</sup> The exact spectra a and c are calculated from the hierarchy equation approach, while the spectra b and d are calculated from the stochastic approach corresponding to the cases a and c, respectively. The red positive-going peaks arise from the  $0 \rightarrow 1 \rightarrow 0$  transition, whereas the blue negative-going peaks arise from the  $0 \rightarrow 1 \rightarrow 2$  transition. The direction of the nodal lines denoted by the dashed lines represents the extent of correlation (or memory effects) between vibrational coherences denoted by  $\omega_1$  and  $\omega_3$ .

by choosing the specific Liouville paths in the energy state model,<sup>1</sup> we have to employ a phase matching transformation for the calculated response functions in the coordinate state case.<sup>41</sup> Note that if we use the plain response function,  $R_R^{(3)}(t_3, t_2, t_1)$  defined by eq 2, in eq 6 instead of  $R_R^{(3)}(t_3, t_2, t_1)$  and  $R_{NR}^{(3)}(t_3, t_2, t_1)$ , we cannot extract the nonrephasing contribution completely and the direction of the nodal line may be different from the true one. Besides the phase matching transformation, one may also eliminate the undesired rephasing contribution by utilizing the Fourier transformation of  $I_C(\omega_3, t_2, \omega_1)$  for  $t_2$  to remove the oscillating contribution in the  $t_2$  period with the frequency  $2\omega_0$ , where  $\omega_0$  is the characteristic frequency of the system.<sup>42,43</sup> The calculated correlation spectra with  $t_2 = 0$  is presented in Figure 3. The red positive peaks and the blue negative peaks correspond to the  $0 \rightarrow 1 \rightarrow 0$  and  $0 \rightarrow 1 \rightarrow 2$  transitions, respectively. The direction of the nodal lines denoted by the dashed lines represents the extent of correlation (memory effects) between the vibrational

coherences of the  $t_1$  and  $t_3$  periods. The direction parallel to the  $\omega_1$  axis is the uncorrelated case, while the direction parallel to the  $\omega_1 = \omega_3$  line is the fully correlated case. The width of the peak parallel to the  $\omega_1 = \omega_3$  direction corresponds to the inhomogeneous broadening, whereas that perpendicular to  $\omega_1 = \omega_3$  is the homogeneous broadening.<sup>44–46</sup> Figure 3a,b shows the 2D correlation IR spectra  $I_C(\omega_3, t_2 = 0, \omega_1)$  of the Morse oscillator in the motional narrowing regime. The correlation is lost even at  $t_2 = 0$ , and the nodal lines are horizontal. Due to the two-quantum transition induced by the SL interaction, the relaxation  $2 \rightarrow 0$  is allowed, while the LL interaction causes mainly one-quantum transition,  $1 \rightarrow 0$  and  $2 \rightarrow 1$ , because of small anharmonicity. As a result, the coherence between  $|1\rangle$  and  $|2\rangle$  is destroyed by both of the two energy relaxation paths,  $2 \rightarrow 1$  and  $2 \rightarrow 0$ , although that between  $|0\rangle$  and  $|1\rangle$  is affected only by the relaxation  $1 \rightarrow 0$ . Hence, the negative peak in the exact case is very different from the stochastic case. Figure 3c,d illustrates the 2D correlation IR spec-

tra for the slow modulation (static) case. In this case, the spectral widths are broadened due to the dephasing (spectral diffusion regime) not due to the energy relaxation. The exact and stochastic results are similar, apart from the small blue shifts caused by the dissipation from the colored noise bath. It is shown that, while the condition  $\beta\hbar\gamma/2 \ll 1$  is met, the signals from a multistate stochastic three-state model agree very well with the signals from a high-frequency Morse potential model with the LL + SL interaction. This is because under such conditions, the characteristic time scale of bath motion ( $\gamma^{-1}$ ) is incompatibly slow compared with that of system one ( $\omega_A^{-1}$ ), and it is hard for the system to dissipate its excess energy to the bath.<sup>18</sup>

### III. Intermolecular Vibrational Modes

While a simple energy state model with the stochastic modulation describes the dephasing fairly well for high-frequency intramolecular vibrational modes, it is not easy to construct a theory based on the energy state representation for low-frequency intermolecular modes, where the thermal excitation and relaxation exchange the population and coherence between a number of low-frequency energy states. As a reference, we present the 2D IR spectra for the intermolecular vibration of liquid molecules calculated from the full molecular dynamics (MD) simulation approach. Three full MD methods have been developed for multidimensional vibrational spectroscopies: (1) the equilibrium approach that computes, exactly or approximately, a nonlinear optical response function expressed in the multiple Poisson brackets of the equilibrium molecular trajectories;<sup>47–49</sup> (2) the nonequilibrium MD (NEMD) approach that performs the 2D spectroscopy experiment on the computer;<sup>50</sup> and (3) the hybrid approach of the first and the second methods.<sup>51</sup> The present result shown in Figure 4 was obtained for HF liquid from the NEMD approach with a backward–forward trajectories sampling method. The details of calculations are described in ref 42. The echo-like peaks caused by the rephasing of the dipole element appear along  $t_1 = t_3$ . We also observed many peaks parallel to  $t_1 = t_3$  corresponding to the interference between the coherences in  $t_1$  and  $t_3$  periods. A similar profile was also found in the simulated 2D IR spectra for the intermolecular vibrational motion of water.<sup>43</sup>

The model calculations for low-frequency vibrations with LL + SL interactions were performed using the hierarchy equations of motion approach.<sup>2,15–17</sup> We found that the MD result was similar to the results in the slow modulation case of the Morse oscillator and harmonic oscillator models with the SL

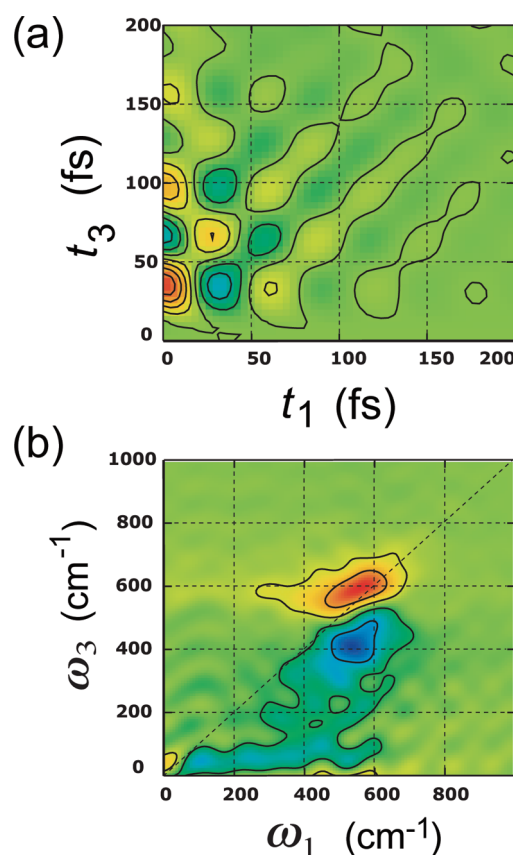


**FIGURE 4.** Two-dimensional IR signals of HF liquid at room temperature obtained from the full MD simulation. Panel a is the time domain signal  $R_3^3(t_3, t_2 = 0, t_1)$ , whereas panel b is the 2D correlation spectrum,  $I_C(\omega_3, t_2 = 0, \omega_1)$ . The red and blue peaks represent the positive and negative contributions, respectively. Reprinted with permission from ref 42. Copyright 2008 American Institute of Physics.

interaction. While the Morse result was closer to the simulation result,<sup>2</sup> here we present the harmonic result since this result is instructive to see the cause of twin positive and negative peaks. In Figure 5, we present the time-domain and 2D correlation spectra for the harmonic potential with the frequency  $\omega_A = 38.7 \text{ cm}^{-1}$  and the system–bath coupling parameters  $\xi_{\text{SL}}^A = 0.1\omega_A$  and  $\gamma_A = 0.1\omega_A$ . The calculation details for the time-domain signal are explained in refs 2, 15, and 17. The 2D correlation spectrum is calculated from the time-domain 2D signal for different  $t_2$  ( $0 \leq t_2 \leq 1.2 \text{ ps}$ ) with Fourier transformation used to remove the oscillating contribution with the frequency  $2\omega_A$ .<sup>42,43</sup>

It is important to notice that in the harmonic oscillator model, the third-order IR response vanishes when the dipole moment is expressed only as a linear function of the molecular coordinate because the contributions to the response function from the different Liouville pathways interfere destructively.<sup>2</sup> If the SL interaction is presented, however, the

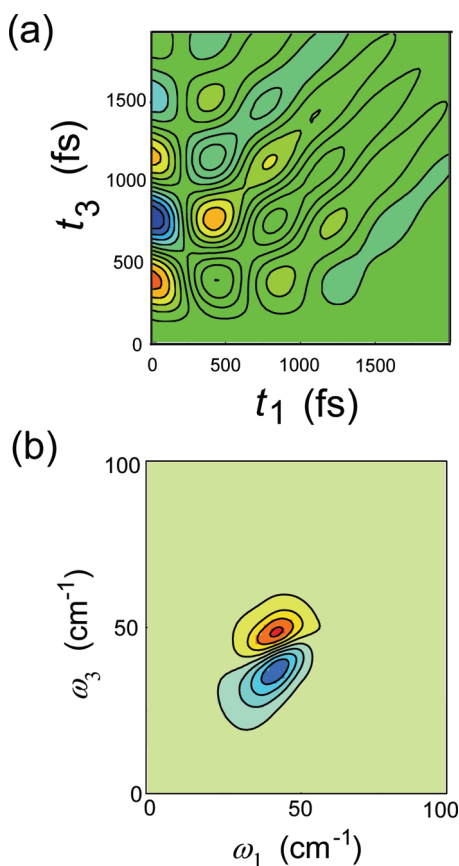


**FIGURE 5.** Two-dimensional IR signals for the low-frequency intermolecular vibrational mode obtained from the hierarchy equation approach.<sup>2,15,17</sup> Panel a is the time-domain signal,  $R_R^{(3)}(t_3, t_2 = 0, t_1)$ , whereas panel b is the correlation spectrum,  $I_C(\omega_3, t_2 = 0, \omega_1)$ .

signal appears since the interference between the different Liouville paths is disturbed due to the frequency fluctuation nature of the SL interaction and the interference being partly ceased. This indicates that the positive and negative peaks of 2D spectrum in Figure 5 arise not from the anharmonicity but from the dephasing. Since the dephasing for the transition  $0 \rightarrow 1 \rightarrow 2$  takes part after the excitation is created by the first and second pulses, the elongation of the negative peak toward the lower frequency of  $\omega_3$  occurs in Figure 5b.

#### IV. Multimode Oscillator System with Anharmonic Coupling

Even in the high-frequency case, an anharmonically coupled multimode system is not easy to handle in the energy-state representation, especially for such a case that each of the modes interacts with different bath environments. Using the hierarchy formalism, we can also study the multimode system based on the coordinate space representation. Here, we show the calculated results for an anharmonically coupled

two-mode system.<sup>19</sup> The two modes A and B are described by the Morse potentials  $U_j(q) = \hbar\omega_j[1 - \exp(-\alpha_j q)]^2/(2\alpha_j^2)$  for  $j = A$  or  $B$  with the parameters  $\omega_A = 1565.7 \text{ cm}^{-1}$ ,  $\omega_B = 1666.7 \text{ cm}^{-1}$ , and  $\alpha_A = \alpha_B = 0.1$ . The anharmonic coupling between the two modes is given by  $U'(\hat{q}_A, \hat{q}_B) = \hbar(g_{AA}^{(3)}q_A^2q_B + g_{BB}^{(3)}q_Aq_B^2)/2$  with  $g_{AA}^{(3)} = g_{BB}^{(3)} = -40 \text{ cm}^{-1}$ . To explore the correlation among different modes through the baths, we consider two cases of system–bath couplings. One is (a) a correlated case that the two modes A and B are coupled to a bath  $B_A$ , and the other is (b) an uncorrelated case that the two modes A and B are independently coupled to the two baths  $B_A$  and  $B_B$ , respectively. Since the LL couplings play minor roles in high-frequency intravibrational motion, we set them to be zero. The SL coupling strengths and inverse noise correlation for  $B_A$  and  $B_B$  are given by  $\xi_{SL}^A = \xi_{SL}^B = 0.4\omega_A$  and  $\gamma_A = \gamma_B = 0.004\omega_A$ , respectively. The 2D IR correlation spectra with  $t_2 = 0$  for the case a is presented in Figure 6a, while that for the case b is illustrated in Figure 6b. The anharmonic coupling between two modes appears as the off-diagonal peaks. The upper positive off-diagonal peaks, for example, correspond to the  $0_A \rightarrow 1_A \sim 1_B \rightarrow 0_B$  transition, while upper negative off-diagonal ones correspond to the  $0_A \rightarrow 1_A \sim 1_B \rightarrow 2_B$  transition for the energy state  $j_A$  or  $j_B$  for mode A or B, respectively. The transition induced by the anharmonic coupling is denoted by “ $\sim$ ”. In the case in Figure 6a, the off-diagonal peaks are tilted parallel to the diagonal peaks, which arise mainly from the rephasing pathways. In the case in Figure 6b, while diagonal peaks for mode A and mode B are similar to those in the case in Figure 6a, the gradient of the off-diagonal peaks in the correlation spectrum is slightly upward. This occurs because the noise on mode A and the noise on mode B are not correlated. These results can be compared with the experimental results obtained by Khalil, Demirdöven, and Tokmakoff.<sup>9</sup>

#### V. Analytical Expressions for Nonlinear Response Functions

Although we can calculate a variety of spectra based upon the coordinate representation by solving the hierarchy equations of motion, this approach requires reasonably strong CPU power to obtain 2D contour maps of signals for different  $t_1$ ,  $t_2$ , and  $t_3$ . Since the molecular motions are more or less harmonic in many vibrational spectroscopy cases, we can treat the anharmonic contribution of vibrations perturbatively. This allows us to reduce the nonlinear response function to a handy analytical form for the system–bath Hamiltonian by carrying out the functional integrals. This is the oldest approach to derive the response functions for multidimen-

sional vibrational spectroscopies such as the fifth-order Raman and third-order IR, which are equivalent to the second-order IR and seventh-order Raman, respectively. The expressions were derived for a harmonic oscillator system with the nonlinear polarizability or dipole,<sup>3,52,53</sup> an anharmonic oscillator,<sup>54–56</sup> a dipolar rotator,<sup>57</sup> and a multimode system with anharmonic couplings<sup>58–60</sup> or dipole–dipole interactions in order to explore the structural changes.<sup>61,62</sup>

Here, we present the nonlinear response functions for the fifth-order Raman and the third-order IR for anharmonically coupled oscillators and display the 2D IR correlation spectra. The Hamiltonian for the system is assumed to be

$$H_A = \sum_i \frac{1}{2} p_i^2 + \frac{1}{2!} \sum_i \omega_i^2 q_i^2 + \frac{1}{3!} \sum_{ijk} g_{ijk}^{(3)} q_i q_j q_k + \frac{1}{4!} \sum_{ijkl} g_{ijkl}^{(4)} q_i q_j q_k q_l \quad (7)$$

If the anharmonicity is weak, we can obtain the fifth-order Raman and third-order IR response functions in terms of anti-symmetric correlation function,  $C_i(t,s) = \langle q_i(t)q_i(s) \rangle / \hbar$  as<sup>58–60</sup>

$$R_{\text{Raman}}^{(5)}(t_2, t_1) = - \sum_{i,j,k,l} g_{ijkl}^{(3)} \int_0^{t_2} d\tau C_i(t_{12}, t_1 + \tau) \times C_j(t_1 + \tau, 0) C_k(t_1 + \tau, t_1) \quad (8)$$

and

$$R_{\text{IR}}^{(3)}(t_3, t_2, t_1) = - \sum_{i,j,k,l} \frac{g_{ijkl}^{(4)} S_{ijkl}}{2} \int_0^{t_3} d\tau C_i(t_{123}, t_{12} + \tau) \times C_j(t_{12} + \tau, 0) C_k(t_{12} + \tau, t_1) C_l(t_{12} + \tau, t_{12}) \quad (9)$$

where  $S_{ijkl}$  is the symmetry factor defined in ref 60. For the LL system–bath interaction with the bath spectral distribution,  $J_i(\omega) \equiv \sum \omega \delta(\omega - \omega_a) = \zeta_i \omega$ , we have the correlation function in the form  $C_i(t,s) = \theta(t-s) \sin[\xi_i(t-s)] / \xi_i$ , where  $\xi_i = (\omega_i^2 - \zeta_i^2/4)^{1/2}$ . In this formalism, the SL interaction plays a more complicated role than LL interaction and could derive the analytical expression only for the linear response function.<sup>12</sup> As we saw in section III, the dissipation part of thermal effect is not essential for the intramolecular vibrations in the static or slow modulation case. Therefore, in the static case, we may include the effects of the vibrational dephasing by adding the Gaussian random variable  $\delta\Omega_i$  to the mode frequency as  $\omega_i + \delta\Omega_i$ , and by averaging the response functions for different  $\xi_i = [(\omega_i + \delta\Omega_i)^2 - \zeta_i^2/4]^{1/2}$ . If we generate the time-dependent stochastic variable  $\delta\Omega_i(t)$ , which satisfies both  $\langle \delta\Omega_i(t) \rangle = 0$  and  $\langle \delta\Omega_i(t) \delta\Omega_j(s) \rangle = f_{ij}(t,s)$ , where  $f_{ij}(t,s)$  is the noise correlation function, we can study spectra for any forms of  $f_{ij}(t,s)$  by using the expressions

$$C_i(t,s) = \theta(t-s) \frac{1}{\xi_i(0)} \sin\left[\int_s^t d\tau \xi_i(\tau)\right] \quad (10)$$

and

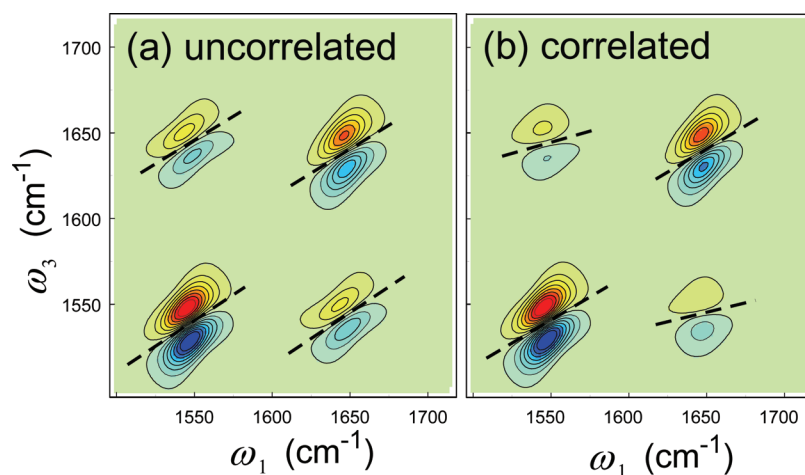


**FIGURE 6.** The 2D correlation IR spectrum,  $I_C(\omega_3, t_2 = 0, \omega_1)$ , for the multimode system with anharmonic mode–mode coupling calculated from the hierarchy equations of motion (taken from ref 19). In panel a, the two modes A and B are coupled to a single bath, whereas in panel b, the two modes A and B are independently coupled to two baths. The widths of the peaks parallel to the  $\omega_1 = \omega_3$  direction represent inhomogeneous broadening, whereas those perpendicular to  $\omega_1 = \omega_3$  represents homogeneous broadening. The twin peaks arise from the  $0 \rightarrow 1 \rightarrow 0$  transition (red) and the  $0 \rightarrow 1 \rightarrow 2$  transition (blue). The diagonal peaks correspond to the mode frequencies of A and B, whereas the off-diagonal peaks correspond to the A to B or B to A coupled modes. The direction of the nodal lines denoted by the dashed lines represents the extent of correlation between vibrational coherences associated with frequencies  $\omega_1$  and  $\omega_3$ . Because the baths are not correlated in panel b, the correlation of the coherence between the two modes is small and the dashed lines on the off-diagonal positions are closer to the horizontal direction than those found in panel a.

$$\xi_i(t) = \sqrt{(\omega_i + \delta\Omega_i(t))^2 - \gamma_i^2/4} \quad (11)$$

where the reduced frequency  $\xi_i(t)$  can be imaginary for  $\langle\omega_i + \delta\Omega_i(t)\rangle < \gamma_i/2$ . It is interesting to notice that the above expressions are quantum mechanical expressions derived from the functional integral approach, but they do not contain the Planck constant. Thus, the expressions eqs 8 and 9 with eqs 10 and 11 are identical in both the quantum and classical cases. This is because the major quantum effect for a nearly harmonic system is the zero point oscillation. Such effect is canceled in vibrational spectroscopy, since we measure not the absolute energy state but the difference between the energy states.

We now examine the expression of the third-order IR response function for a multimode system with anharmonicity  $U_A(q_A) = g_A^{(4)}q_A^4$ ,  $U_B(q_B) = g_B^{(4)}q_B^4$ , and  $U'(q_A, q_B) = g_{AABB}^{(4)}q_A^2q_B^2$ . We set the oscillators parameters as  $\omega_A = 1550 \text{ cm}^{-1}$ ,  $\omega_B = 1650 \text{ cm}^{-1}$ ,  $g_A^{(4)} = g_B^{(4)} = g_{AABB}^{(4)}$ . The LL interactions for the A and B modes are set by  $\zeta_A = 2.6 \times 10^{-3}\omega_A$  and  $\zeta_B = 3.0 \times 10^{-3}\omega_B$ , respectively. The correlation functions of stochastic modulation are assumed to be  $f_i(t) = \Delta_i^2 \exp[-\gamma_{SL}^i t]$ . Note that although here we consider the Gaussian–Markovian noise as the frequency modulation, we can handle any noise including the non-Gaussian and non-Markovian noise if we can generate a sequence of the noise  $f_i(t)$  numerically. We also assume the two independent heat baths for the mode A and B to have different amplitudes,  $\Delta_A = 5.2 \times 10^{-2}\omega_A$  and  $\Delta_B = 3.8 \times 10^{-2}\omega_B$ , and noise correlations,  $\gamma_{SL}^A = 0.25\omega_A$  and  $\gamma_{SL}^B = 0.30\omega_B$ , respectively. To have the correlation spectra from full response function, we extract the undesired rephasing contribution, which oscillates as the function of  $t_2$  as  $\cos[\int_0^{t_2}(\xi_i(t) + \xi_j(t)) dt]$ , from the analytical expression. The calculated correlation spectrum is shown in Figure 7. Since the amplitude and correlation time of the A and B modes are different, the widths of the diagonal peaks are different. While the case in Figure 3 assumed cubic anharmonic coupling, the present case considers a quartic anharmonic one. We found that if the amplitude of the stochastic fluctuation  $\delta\Omega_i(t)$  is large and the noise correlation time  $1/\gamma_{SL}^i$  is short, the nodal lines tend to be horizontal reflecting the loss of the correlation.

## VI. Conclusions

Multidimensional vibrational spectra can be conveniently analyzed by a system–bath model in the coordinate representation with nonlinear system–bath interactions. As an application of the oscillator model, we calculate the correlation spectra for inter- and intramolecular vibrational motions. We explore the validity of the energy state model with the stochastic energy state modulation by comparing the calculated

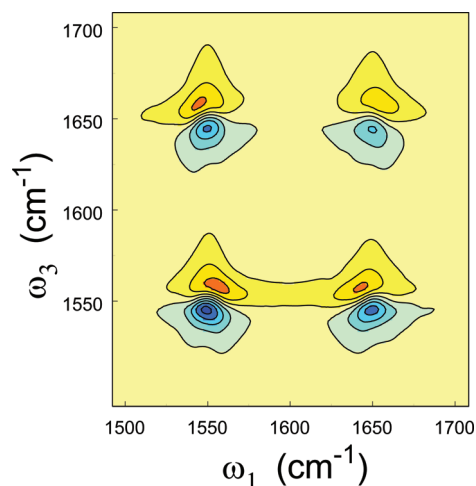


**FIGURE 7.** Two dimensional correlation IR spectra,  $I_c(\omega_3, t_2 = 0, \omega_1)$ , for the multimode system with quartic anharmonicity calculated from eq 9.<sup>60</sup> Effects of vibrational dephasing are taken into account by introducing the numerically generated colored noise in the resonant frequencies and by averaging the response function over the noise sequence.

multidimensional IR correlation spectra for the high-frequency intramolecular vibrational mode. It was found that while the energy state model worked very well in the slow modulation case, it failed to explain the profile of the signal in the fast modulation case in Figure 3a, where the system reached the thermal equilibrium state quickly.

Multimode systems attached to a single bath and multiple baths are employed to demonstrate the role of the system–bath coherence in the multidimensional spectroscopies. The handy analytical expressions are also shown to be useful if the stochastic modulation is slow enough. Although we limit our discussions for the oscillatory motion in this Account, we can easily apply our coordinate-based approach to the chemical reaction system<sup>63,64</sup> and photodissociation system with electrically excitation states.<sup>65</sup> Since we describe the system in the coordinate space, the classical and quantal correspondences can be easily studied by replacing the quantal equations of motion with the classical ones. To study the multidimensional spectra for such complicated systems as a complex liquid system and a biomolecular system with a MD approach, one needs to know the limitation of the classical simulation. Our model calculations for the quantum and classical cases allow us to confirm the applicability of MD approach. We should also mention that although we regard the coordinate as the molecular coordinate to have the dynamics for anharmonic potentials, we may use the same framework to explore the free energy landscape by means of multidimensional spectroscopies if we regard the coordinates as macroscopic variables.<sup>66</sup> Such approach must be a valu-



able method for analyzing spectra obtained by multidimensional terahertz spectroscopy, where the collective motions play a major role.<sup>59</sup>

*Y.T. is thankful for the financial support from a Grant-in-Aid for Scientific Research B19350011 from the Japan Society for the Promotion of Science.*

## BIOGRAPHICAL INFORMATION

**Yoshitaka Tanimura** received his Ph.D. from Keio University in 1989. He was at the University of Illinois and the University of Rochester as a postdoctoral fellow. Then he spent nine years as associate professor at the Institute for Molecular Science before joining the faculty at Kyoto University in 2003. Research in his group is broadly concerned with the dynamic theory of processes of chemical interest in condensed matter.

**Akihito Ishizaki** conducted his doctoral research under the guidance of Prof. Yoshitaka Tanimura at Department of Chemistry, Kyoto University, from which he earned his Ph.D. in 2008. He is currently a JSPJ postdoctoral fellow in the laboratory of Prof. Graham R. Fleming at Department of Chemistry, University of California, Berkeley. His research interest includes theoretical studies of quantum dynamic phenomena in chemical and biological systems.

## FOOTNOTES

\* To whom correspondence should be addressed. E-mail: tanimura@kuchem.kyoto-u.ac.jp.

<sup>†</sup> Present address: Department of Chemistry, University of California Berkeley, Berkeley, CA 94720.

## REFERENCES

- Mukamel, S. *Principles of Nonlinear Optical Spectroscopy*; Oxford University Press, New York, 1995.
- Tanimura, Y. Stochastic Liouville, Langevin, Fokker-Planck, and master equation approaches to quantum dissipative systems. *J. Phys. Soc. Jpn.* **2006**, *75*, 082001.
- Tanimura, Y.; Mukamel, S. Two-dimensional femtosecond vibrational spectroscopy of liquids. *J. Chem. Phys.* **1993**, *99*, 9496–9511.
- Kubarych, K. J.; Milne, C. L.; Lin, S.; Astinov, V.; Miller, R. J. D. *J. Chem. Phys.* **2002**, *116*, 2016–2042.
- Kaufman, L. J.; Heo, J.; Ziegler, L. D.; Fleming, G. R. *Phys. Rev. Lett.* **2002**, *88*, 207402.
- Li, Y. L.; Huang, L.; Dwayne Miller, R. J.; Hasegawa, T.; Tanimura, Y. Two-dimensional fifth-order Raman spectroscopy of liquid formamide: Experiment and theory. *J. Chem. Phys.* **2008**, *128*, 234507.
- Hamm, P.; Lim, M.; Hochstrasser, R. M. Structure of the amide I band of peptides measured by femtosecond nonlinear-infrared spectroscopy. *J. Phys. Chem. B* **1998**, *102*, 6123–6138.
- Asplund, M. C.; Zanni, M. T.; Hochstrasser, R. M. Two dimensional infrared spectroscopy of peptides by phase-controlled femtosecond vibrational photon echoes. *Proc. Natl. Acad. Sci. U.S.A.* **2000**, *97*, 8219–8224.
- Khalil, M.; Demirdöven, N.; Tokmakoff, A. Coherent 2D IR spectroscopy: Molecular structure and dynamics in solution. *J. Phys. Chem. A* **2003**, *107*, 5258–5279.
- Kraemer, D.; Cowan, M. L.; Paarmann, A.; Huse, N.; Nibbering, E. T. J.; Elsaesser, T.; Miller, R. J. D. Temperature dependence of the two-dimensional infrared spectrum of liquid H<sub>2</sub>O. *Proc. Natl. Acad. Sci. U.S.A.* **2008**, *105*, 437–442.
- Straus, J. B.; Liorente, J. M.; Voth, G. A. Manifestations of spatially dependent friction in classical activated rate processes. *J. Chem. Phys.* **1991**, *98*, 4082–4097.
- Okumura, K.; Tanimura, Y. Two-time correlation functions of a harmonic system non-bilinearly coupled to a heat bath: The spontaneous Raman spectroscopy. *Phys. Rev. E* **1997**, *56*, 2747–2750.
- Ghosh, P. K.; Barik, D.; Ray, D. S. Inhomogeneous quantum diffusion and decay of a meta-stable state. *Phys. Lett. A* **2007**, *361*, 201–211.
- Oxtoby, D. W. Dephasing of molecular vibrations in liquids. *Adv. Chem. Phys.* **1979**, *40*, 1–48.
- Tanimura, Y.; Steffen, T. Two dimensional spectroscopy for harmonic vibrational modes with nonlinear system-bath interactions: II. Gaussian-Markovian case. *J. Phys. Soc. Jpn.* **2000**, *69*, 4095–4106.
- Kato, T.; Tanimura, Y. Vibrational spectroscopy of a harmonic oscillator system nonlinearly coupled to a heat bath. *J. Chem. Phys.* **2002**, *117*, 6221–6234.
- Kato, T.; Tanimura, Y. Two-dimensional Raman and infrared vibrational spectroscopy for a harmonic oscillator system nonlinearly coupled with a colored noise bath. *J. Chem. Phys.* **2004**, *120*, 260–271.
- Ishizaki, A.; Tanimura, Y. Modeling vibrational dephasing and energy relaxation processes of intermolecular anharmonic modes for multidimensional infrared spectroscopies. *J. Chem. Phys.* **2006**, *125*, 084501.
- Ishizaki, A.; Tanimura, Y. Dynamics of multimode system coupled to multiple heat baths probed by two-dimensional infrared spectroscopy. *J. Phys. Chem. A* **2007**, *111*, 9269–9276.
- Hamm, P.; Lim, M.; Hochstrasser, R. M. Non-Markovian dynamics of the vibrations of ions in water from femtosecond infrared three-pulse photon echoes. *Phys. Rev. Lett.* **1998**, *81*, 5326–5329.
- Everitt, K. F.; Geva, E.; Skinner, J. L. Determining the solvation correlation function from three-pulse photon echoes in liquids. *J. Chem. Phys.* **2001**, *114*, 1326–1335.
- Cho, M. Nonlinear response functions for the three-dimensional spectroscopies. *J. Chem. Phys.* **2001**, *115*, 4424–4437.
- Fourkas, J. T. Higher-order optical correlation spectroscopy in liquids. *Annu. Rev. Phys. Chem.* **2002**, *53*, 17–40.
- Merchant, K. A.; Noid, W. G.; Thompson, D. E.; Akiyama, R.; Loring, R. F.; Fayer, M. D. Structural assignments and dynamics of the A substates of MbCO: Spectrally resolved vibrational echo experiments and molecular dynamics simulations. *J. Phys. Chem. B* **2003**, *107*, 4–7.
- Sanda, F.; Mukamel, S. Stochastic simulation of chemical exchange in two dimensional infrared spectroscopy. *J. Chem. Phys.* **2006**, *125*, 014507.
- Zhuang, W.; Hayashi, T.; Mukamel, S. *Angew. Chem., Int. Ed.* **2009**, in press.
- Jansen, T. L. C.; Ruszel, W. M. Motional narrowing in the time-averaging approximation for simulating two-dimensional nonlinear infrared spectra. *J. Chem. Phys.* **2008**, *128*, 214501.
- Hanna, G.; Geva, E. Computational study of the one and two dimensional infrared spectra of a vibrational mode strongly coupled to its environment: Beyond the cumulant and Condon approximations. *J. Phys. Chem. B* **2008**, *112*, 12991–13004.
- Tanimura, Y.; Kubo, R. Time evolution of a quantum system in contact with a nearly Gaussian-Markovian noise bath. *J. Phys. Soc. Jpn.* **1989**, *58*, 101–114.
- Tanimura, Y.; Wolynes, P. G. Quantum and classical Fokker-Planck equations for a Gaussian-Markovian noise bath. *Phys. Rev. A* **1991**, *43*, 4131–4142.
- Tanimura, Y. Nonperturbative expansion method for a quantum system coupled to a harmonic-oscillator bath. *Phys. Rev. A* **1990**, *41*, 6676–6687.
- Chernyak, V.; Mukamel, S. Collective coordinates for nuclear spectral densities in energy transfer and femtosecond spectroscopy of molecular aggregates. *J. Chem. Phys.* **1996**, *105*, 4565–4583.
- Mo, Y.; Xu, R. X.; Cui, P.; Yan, Y. J. Correlation and response functions with non-Markovian dissipation: A reduced Liouville-space theory. *J. Chem. Phys.* **2005**, *122*, 084115.
- Ishizaki, A.; Tanimura, Y. Quantum dynamics of a system strongly coupled to a low temperature colored noise bath: Reduced hierarchy equations approach. *J. Phys. Soc. Jpn.* **2005**, *74*, 3131–3134.
- Ishizaki, A.; Tanimura, Y. Nonperturbative-nonMarkovian quantum master equation approach: Validity and limitation to calculate nonlinear response functions. *Chem. Phys.* **2008**, *347*, 185–193.
- Ernst, R. R.; Bodenhausen, G.; Wokaun, A. *Principles of Nuclear Magnetic Resonance in One and Two Dimensions*; Oxford University Press: Oxford, U.K., 1987.
- Hybl, J. D.; Ferro, A. A.; Jonas, D. M. *J. Chem. Phys.* **2001**, *115*, 6606–6622.
- Ge, N.-H.; Zanni, M. T.; Hochstrasser, R. M. Effects of vibrational frequency correlations on two-dimensional infrared spectra. *J. Phys. Chem. A* **2002**, *106*, 962–972.
- Khalil, M.; Demirdöven, N.; Tokmakoff, A. Obtaining absorptive line shapes in two-dimensional infrared vibrational correlation spectra. *Phys. Rev. Lett.* **2003**, *90*, 047401.
- Venkatramani, R.; Mukamel, S. Correlated line broadening in multidimensional vibrational spectroscopy. *J. Chem. Phys.* **2002**, *117*, 11089–11101.
- Kato, T.; Tanimura, Y. Multi-dimensional vibrational spectroscopy measured from different phase-matching conditions. *Chem. Phys. Lett.* **2001**, *341*, 329–337.

- 42 Hasegawa, T.; Tanimura, Y. Nonequilibrium molecular dynamics simulations with a backward-forward trajectories sampling for multidimensional infrared spectroscopy of molecular vibrational modes. *J. Chem. Phys.* **2008**, *128*, 064511.
- 43 Yagasaki, T.; Saito, S. Ultrafast intermolecular dynamics of liquid water: A theoretical study on two-dimensional infrared spectroscopy. *J. Chem. Phys.* **2008**, *128*, 154521.
- 44 Okumura, K.; Tokmakoff, A.; Tanimura, Y. Two-dimensional line shape analysis of photon echo signal. *Chem. Phys. Lett.* **1999**, *314*, 488–495.
- 45 Lazonder, K.; Pshenichnikov, M. S.; Wiersma, D. A. Easy interpretation of optical two-dimensional correlation spectra. *Opt. Lett.* **2006**, *31*, 3354–3356.
- 46 Cho, M. Coherent two-dimensional optical spectroscopy. *Chem. Rev.* **2008**, *108*, 1331–1418.
- 47 Ma, A.; Stratt, R. M. Fifth-order Raman spectrum of an atomic liquid: Simulation and instantaneous-normal-mode calculation. *Phys. Rev. Lett.* **2000**, *85*, 1004–1007.
- 48 Saito, S.; Ohmine, I. Off-resonant fifth-order response function for two-dimensional Raman spectroscopy of liquids CS<sub>2</sub> and H<sub>2</sub>O. *Phys. Rev. Lett.* **2002**, *88*, 207401.
- 49 Nagata, Y.; Tanimura, Y. Two-dimensional Raman spectra of atomic solids and liquids. *J. Chem. Phys.* **2006**, *124*, 024508.
- 50 Jansen, T. L. C.; Snijders, J. G.; Duppen, K. The third- and fifth-order nonlinear Raman response of liquid CS<sub>2</sub> calculated using a finite field nonequilibrium molecular dynamics method. *J. Chem. Phys.* **2000**, *113*, 307–311.
- 51 Hasegawa, T.; Tanimura, Y. Calculating fifth-order Raman signals for various molecular liquids by equilibrium and nonequilibrium hybrid molecular dynamics simulation algorithms. *J. Chem. Phys.* **2006**, *125*, 074512.
- 52 Hahn, S.; Park, K.; Cho, M. Two-dimensional vibrational spectroscopy. I. Theoretical calculation of the nonlinear Raman response function of CHCl<sub>3</sub>. *J. Chem. Phys.* **1999**, *111*, 4121–4130.
- 53 Park, K.; Cho, M.; Hahn, S.; Kim, D. Two-dimensional vibrational spectroscopy. II. Ab initio calculation of the coherent 2D infrared response function of CHCl<sub>3</sub> and comparison with the 2D Raman response function. *J. Chem. Phys.* **1999**, *111*, 4131–4139.
- 54 Okumura, K.; Tanimura, Y. The  $(2n+1)$ th-order off-resonant spectroscopy from the  $(n+1)$ th-order anharmonicities for molecular vibrational modes in the condensed phase. *J. Chem. Phys.* **1997**, *106*, 1687–1698.
- 55 Okumura, K.; Tanimura, Y. Femtosecond two-dimensional spectroscopy from anharmonic vibrational modes of molecules in the condensed phase. *J. Chem. Phys.* **1997**, *107*, 2267–2283.
- 56 Park, K.; Cho, M. Time- and frequency-resolved coherent two-dimensional IR spectroscopy: Its complementary relationship with the coherent two-dimensional Raman scattering spectroscopy. *J. Chem. Phys.* **1998**, *109*, 10559–10569.
- 57 Suzuki, Y.; Tanimura, Y. Two-dimensional spectroscopy for a two-dimensional rotator coupled to a Gaussian-Markovian noise bath. *J. Chem. Phys.* **2003**, *119*, 1650–1660.
- 58 Okumura, K.; Tanimura, Y. Sensitivity of two-dimensional fifth-order Raman response to the mechanism of vibrational mode-mode coupling in liquid molecules. *Chem. Phys. Lett.* **1997**, *278*, 175–183.
- 59 Okumura, K.; Tanimura, Y. Two-dimensional THz spectroscopy of liquids: nonlinear vibrational response to a series of THz laser pulses. *Chem. Phys. Lett.* **1998**, *295*, 298–304.
- 60 Okumura, K.; Jonas, D. M.; Tanimura, Y. Two-dimensional spectroscopy and the harmonically coupled anharmonic oscillators. *Chem. Phys.* **2001**, *266*, 237–250.
- 61 Okumura, K.; Tokmakoff, A.; Tanimura, Y. Structural information from two-dimensional fifth-order Raman spectroscopy. *J. Chem. Phys.* **1999**, *111*, 492–503.
- 62 Kim, H.-D.; Tanimura, Y. Multi-dimensional infrared spectroscopy for molecular vibrational modes with dipolar interactions, anharmonicity and nonlinearity of dipole moments and polarizability elements. *J. Chem. Phys.* **2005**, *123*, 224310.
- 63 Kühn, O.; Tanimura, Y. Two-dimensional vibrational spectroscopy of a double minimum system in a dissipative environment. *J. Chem. Phys.* **2003**, *119*, 2155–2164.
- 64 Ishizaki, A.; Tanimura, Y. Multidimensional vibrational spectroscopy for tunneling processes in a dissipative environment. *J. Chem. Phys.* **2005**, *123*, 014503.
- 65 Tanimura, Y.; Maruyama, Y. Gaussian-Markovian quantum Fokker-Planck approach to nonlinear spectroscopy of a displaced Morse potentials system: dissociation, predissociation and optical Stark effects. *J. Chem. Phys.* **1997**, *107*, 1779–1793.
- 66 Suzuki, Y.; Tanimura, Y. Exploring a free energy landscape by means of multidimensional infrared and terahertz spectroscopies. *J. Chem. Phys.* **2008**, *128*, 164501.